Mutations in the N-terminal Flanking Region of the Blue-light Sensing Domain LOV2 Disrupt its Repressive Activity on the Kinase Domain in the *Chlamydomonas* Phototropin*

Yusuke Aihara[1], Takaharu Yamamoto[2], Koji Okajima[3], Kazuhiko Yamamoto[1], Tomomi Suzuki[1], Satoru Tokutomi[3], Kazuma Tanaka[2] and Akira Nagatani[1]

[1]From the Department of Botany, Graduate School of Science, Kyoto University, Kyoto 606-8502, Japan; [2]The Division of Molecular Interaction, Institute for Genetic Medicine, Hokkaido University Graduate School of Life Science, Sapporo 060-0815, Japan; [3] The Department of Biological Sciences, Graduate School of Science, Osaka Prefecture University, Osaka 599-8531, Japan

*Running title: *Mutations in the N-terminal flanking region of LOV2 in CrPHOT*

To whom correspondence should be addressed: Akira Nagatani, Tel.: +81 75-753-4123; fax: +81 75-753-4126; e-mail: nagatani@physiol.bot.kyoto-u.ac.jp.

Keywords: phototropin; LOV; pseudolit activity

Background: A plant photoreceptor "phototropin" is a light-dependent kinase containing the LOV photosensory domains.
Results: Mutations in the N-terminal flanking region of LOV2 elevate kinase activity in darkness.
Conclusion: The N-terminal flanking region is involved in intramolecular signaling from LOV2 to the kinase domain.
Significance: This work provides insights into how the LOV domain can activate the kinase domain intramolecularly.

SUMMERY

Phototropin is a light-regulated kinase that mediates a variety of photoresponses such as phototropism, chloroplast positioning and stomata opening in plants to increase the photosynthetic efficiency. Blue-light stimulus first induces local conformational changes in the chromophore-bearing Light-Oxygen and Voltage 2 (LOV2) domain of phototropin, which in turn activates the serine/threonine (Ser/Thr) kinase domain in the C-terminus. To examine the kinase activity of full-length phototropin conventionally, we employed the budding yeast *Saccharomyces cerevisiae*. In this organism, Ser/Thr kinases (Fpk1p and Fpk2p) that show high sequence similarity to the kinase domain of phototropins exist. First, we demonstrated that the phototropin from *Chlamydomonas reinhardtii* (*Cr*PHOT) could complement loss of Fpk1p and Fpk2p to allow cell growth in yeast. Furthermore, this reaction was blue-light dependent, indicating that *Cr*PHOT was indeed light-activated in yeast cells. We then applied this system to a large-scale screening for amino acid substitutions in *Cr*PHOT that elevated the kinase activity in darkness. Consequently, we identified a cluster of mutations located in the N-terminal flanking region of LOV2 (R199C, L202L, D203N/G/V, L204P, T207I and R210H). An *in vitro* phosphorylation assay confirmed that these mutations substantially reduced the repressive activity of LOV2 on the kinase domain in darkness. Furthermore, biochemical analyses of the representative T207I mutant demonstrated that the mutation affected neither spectral nor multimerization properties of *Cr*PHOT. Hence, the N-terminal flanking region of LOV2, as is the case with the C-terminal flanking Jα region, appears to play a crucial role in the regulation of kinase activity in phototropin.

To sense and respond to a fluctuating light environment, plants have evolved several classes of photoreceptor molecules that convert visible light stimuli into biological signals. Phototropin (PHOT) is a blue-light (BL) receptor, which is widely conserved in the plant kingdom (1). Most terrestrial plants possess two isoforms of phototropin designated PHOT1 and PHOT2. In *Arabidopsis thaliana* (*At*), PHOT1 and PHOT2 have redundant and distinct functions to mediate responses, such as phototropism (2,3), chloroplast movement (4,5), stomatal opening (6) and leaf photomorphogenesis (7,8) to optimize photosynthesis. On the other hand,

the unicellular green alga *Chlamydomonas reinhardtii* (*Cr*) possesses a single phototropin homologue (*Cr*PHOT), which has been proposed to regulate sexual differentiation (9,10) and the expression several photosynthetic genes. Interestingly, *Cr*PHOT is fully functional in *Arabidopsis*, suggesting that the basic mechanism of phototropin signal transduction is highly conserved (11).

Phototropins are BL-dependent Ser/Thr protein kinases that share well-conserved structural properties. The kinase domain belongs to the AGC VIII subfamily (protein kinases A, G and C) (12). Autophosphorylation of a conserved serine residue at the activation loop of the kinase domain is prerequisite for its physiological activity (13,14). To date, little is known about authentic phosphorylation substrates for phototropins. Recently however, auxin efflux transporter ATP-BINDING CASSETTE B19 (ABCB19) has been reported as a putative endogenous substrate in *Arabidopsis* (15).

Besides the kinase domain, phototropin contains two N-terminal Light-Oxygen and Voltage (LOV) domains, designated LOV1 and LOV2. The LOV domains, which are members of the Per-ARNT-Sim (PAS) domain superfamily, noncovalently bind flavin mononucleotide (FMN) as chromophores (16). Because the kinase fragment lacking LOV domains displays constitutive activity both *in planta* (17) and *in vitro* (18), LOV domains appear to intrinsically suppress kinase activity in darkness.

Upon BL absorption, a covalent adduct is formed between the FMN and a conserved cysteine residue within each LOV domain (19,20). Consequently, reorganization of the hydrogen bond network takes place in the FMN binding pocket (21,22). Inactivation of LOV domains by site-directed mutagenesis indicates that LOV2 plays a predominant role in regulating the kinase activity (18,23,24), whereas the role of LOV1 is limited to modulate photosensitivity (18). An NMR analysis of *Avena* PHOT1 has revealed an amphipathic α-helix, Jα, which is attached to the C-terminus of the LOV2 core domain (25). The Jα helix changes its structure in response to a light stimulus. Namely, it detaches from the LOV2 core (25) and unfolds (26,27). The prominent role of the Jα helix in the regulation of kinase activity has been evidenced by site-directed mutagenesis in *Arabidopsis* PHOT1. An amino acid substitution that disrupts the LOV2-Jα interaction leads to constitutive activation of the kinase *in vitro* (28).

More recently, the crystallographic analysis of *Avena* PHOT1 LOV2 has suggested that not only the C-terminal Jα but also the N-terminal flanking region display a light-induced structural change (22). These structural changes are presumed to disrupt the inhibitory interaction of LOV2 with the kinase domains. Accordingly, photoreversible contact/separation between the LOV2 and the kinase domains has been suggested by small-angle X-ray scattering (SAXS) in a LOV2-linker-kinase fragment of *Arabidopsis* PHOT2 (29).

Besides the site-directed mutagenesis approach based on structural information, a random-mutagenesis approach utilizing *Escherichia coli* (*E. coli*) as a host has been successfully applied to uncover amino acid residues involved in the photochemistry of LOV2 in *Avena* PHOT1 (30). Although this method is quite effective for identifying spectral mutants in the LOV domains, it is not applicable for screening mutants that are altered in the photoregulation of the kinase activity. This is because no convenient way to assess the kinase activity of phototropin in *E. coli* exists.

In this study, we developed a new yeast experimental system in which *Cr*PHOT triggered cell growth depending on its kinase activity. We then applied this method to screen for mutations that disrupt repression of the kinase domain. Consequently, we revealed that the N-terminal flanking region of LOV2 is important for the suppression of kinase activity in darkness.

EXPERIMENTAL PROCEDURES

Media and Growth Conditions for Yeast–Yeast strains were cultured in YPDA rich medium (1% yeast extract, 2% bacto-peptone, 2% glucose, and 0.01% adenine). Strains carrying plasmids were selected in synthetic medium (SD) containing the required nutritional supplements (31). When appropriate, 0.5% casamino acids were added to SD medium without uracil (SDA-Ura). For induction of the *GAL1* promoter, 3% galactose and 0.2% sucrose were added as carbon sources instead of glucose (YPGA and SGA-Ura). Growth sensitivity to duramycin was examined on YPDA plates containing 10 μM duramycin (Sigma). Blue (peak at 470 nm) and red (peak at 660 nm) light-emitting-diode panels (ISL-150X150 series; CCS, Tokyo, Japan) were used as light sources.

Strains and Plasmids–*Saccharomyces cerevisiae* strains KKT330 (MATa *ura3Δ his3Δ1 leu2Δ0 HIS3MX6::*P_{GAL1}*-CDC50 fpk1Δ::HphMX4 fpk2Δ::KanMX6*, designated hereafter as P_{GAL1}*-CDC50 fpk1*Δ *fpk2*Δ) and YKT1638 (MATa

ura3Δ his3Δ1 leu2Δ0 fpk1Δ::HphMX4 fpk2Δ::KanMX6, designated hereafter as *fpk1*Δ *fpk2*Δ) were used for growth assays (32). The *E coli* strains DH5α and BL21 were used for plasmid construction and expression of recombinant proteins, respectively.

For yeast assays, pRS416-AtPHOT1, pRS416-AtPHOT2, and pRS416-CrPHOT were constructed as follows. The coding regions of *PHOT1* and *PHOT2* from *Arabidopsis* and *PHOT* from *Chlamydomonas* were amplified by PCR and cloned into BamI/SalI site of pRS416 (33) to allow constitutive expression of phototropins tagged with N-terminal two tandem repeats of the influenza virus hemagglutinin epitope (2HA) under the control of the *TPI1* promoter. Site-directed mutations were introduced by using the QuickChange site-directed mutagenesis kit (Strategene) in accordance with the instructions of the supplier. All amino acid changes were verified by DNA sequencing. For over-expression of *Cr*PHOT protein in *E coli*, pET28a-CrPHOT was constructed as follows. Wild-type (WT) and mutant *PHOT* were amplified from pRS416-CrPHOT and cloned into NdeI/SalI sites of pET28a plasmid vector (Novagen) to allow expression of *Cr*PHOT with an N-terminal histidine tag, which was composed of 20 residues including six histidine residues.

Immunoblot Analysis–Protein extraction from yeast was performed as described (34). Immunoblot analysis was performed essentially as described previously (11). The same amount of protein extracts were run on 10.0% SDS-PAGE and blotted onto nitrocellulose membrane. Rat anti-HA monoclonal antibody (Roche) and alkaline phosphatase-conjugated anti-rat IgG antibody (Promega) were used.

Yeast Growth Assay–The cells were grown in liquid SGA-Ura medium to A_{600} 0.6-0.8, harvested by centrifugation and resuspended into sterile water, resulting in an A_{600} of 0.1. Serial 5-time dilutions were then prepared for loading 10 μl each of the diluted cell suspension onto a plate with SGA-Ura or SDA-Ura medium. The plates were then placed under different light conditions.

PCR-Based Random Mutagenesis and Mutant Screening for Pseudolit Phenotype–Error-prone PCR libraries of the N-terminal (1-1399) and C-terminal (1179-2136) moieties of *CrPHOT* flanked by sequences from the pRS416 vector (approximately 150 bp) were generated from the pRS416-CrPHOT using the Diversity PCR random mutagenesis kit (Clontech). The primer sequences are listed below:

5'GTGAACTTGCAACATTTACTATTTTCCC
(pRS416-fw for the N-terminal library)
5'TCGGTCTGGATGGTGCAGTACAG
(CrPHOT-1399rv for the N-terminal library)
5'CTACCAGGCGCTGCTGCAGCTG
(CrPHOT-1179fw for the C-terminal library)
5'AAAGCGGGCAGTGAGCGCAACGC
(pRS416-rv for the C-terminal library)

Final concentrations of 320 μM $MnSO_4$ and 16 μM dGTP were chosen for the PCR reaction to adjust the mutagenesis frequency to 1.5 mutation/kb.

The pRS416-CrPHOT plasmid was digested with BamHI/NruI and SalI/NruI to remove the sequence encoding the N-terminal and C-terminal moieties, respectively. The N- or C-terminal PCR fragments and a pRS416-CrPHOT derived vector lacking the corresponding part of *CrPHOT* were mixed and transformed into the P_{GAL1}-*CDC50 fpk1Δ fpk2Δ* yeast strain, so that homologous recombination generated a vector containing mutagenized *PHOT*. The yeast strain was then plated on SDA-Ura agar, and incubated in the dark at 28°C for 60 h. The growing colonies were isolated. Among isolated colonies, candidates were randomly selected, and plasmids were rescued using Wizard prep (Promega) according to the instructions in the DUALhybrid Kit (Dualsystems Biotech). The candidate plasmids were sequenced in the mutagenized moieties. The second growth assay was performed by repeating the assays using the purified plasmids.

Expression and Purification of Recombinant Proteins–6His-tagged full-length *Cr*PHOT and N-terminal fragment of *Arabidopsis* PHOT1 (*At*P1-Nt) were prepared from *E. coli* according to the protocols used for LOV2-linker-kinase fragment preparation (35) with minor modifications. The *E. coli* cells were lysed with a FRENCH pressure cell (Thermo Fisher scientific) in a buffer containing 20 mM HEPES-NaOH (pH 7.8), 500 mM NaCL, and 1mM PMSF. The purification was performed at 0-4°C under a dim red light. The centrifugation supernatant of the lysate was subjected to Ni^{2+}-ion affinity chromatography (QIAGEN). The *At*P1-Nt were then desalted by using HiTrap Desalting (GE healthcare) and stored at -80 °C.

The *Cr*PHOT protein was further purified via size exclusion column chromatography (Sephacryl HR 200, GE Healthcare) in a buffer containing 100 mM NaCl, 1 mM EGTA and 20 mM Tris-HCl (pH 7.8). Glycerol was added to the eluted *Cr*PHOT to a final concentration of 10% (v/v). The phosphorylation levels of the products after purification were

examined by Pro-Q Diamond phosphoprotein gel-stain (Invitrogen) according to the manufacturer's instruction if necessary.

For the spectral analysis, the above sample was further purified using an anion-exchange RESOURCE Q column (GE Healthcare) equilibrated with a buffer containing 10% (v/v) glycerol, 1mM EGTA, and 20 mM Tris-HCl (pH 7.8). The *Cr*PHOT fraction that did not bind to the RESOURCE Q column was collected and concentrated by ultrafiltration using the Amicon Ultra K15 (MILLIPORE). The purity of *Cr*PHOT in each step was examined by SDS-PAGE.

In Vitro Phosphorylation Assays–The phosphorylation assay was performed under dim green light (18,35). *Cr*PHOT and *At*P1-Nt polypeptides were incubated at 30°C in a kinase reaction mixture containing 20 mM Tris-HCl (pH 7.8), 100mM NaCl, 10% glycerol, 10 mM MgCl, 500 μM ATP and 60 kBq of [γ-32P]ATP. The reaction was terminated by the addition of concentrated SDS-PAGE sample buffer followed by boiling for 3 min. Then, the samples were run on SDS-PAGE to visualize phosphorylation bands using an imaging plate and a bioimaging analyzer (FLA2000, Fuji, Japan). The molecular masses of phosphorylated proteins were estimated by Coomassie brilliant blue (CBB) staining with reference to molecular weight standard samples (Sigma).

Spectral Analyses and Size-Exclusion Chromatography–The absorption spectra of *Cr*PHOT under BL illumination and the time course of absorption changes during thermal decay from the cysteinyl adduct state to the dark-adapted state were measured essentially as described previously (35), at 20°C and pH 7.8. The molecular weight of *Cr*PHOT was estimated by size-exclusion chromatography using a Superdex 200 pg Hi-Load column (GE Healthcare) and the kinase reaction buffer as previously described (35).

RESULTS

Complementation of fpk1Δ fpk2Δ and cdc50Δ Synthetic Lethality in Saccharomyces cerevisiae by Chlamydomonas PHOT in a BL-Dependent Manner –To establish an experimental system that can easily and quickly assess the light-dependent kinase activity of phototropin, we employed *Saccharomyces cerevisiae*, in which the protein-kinases named flippase-kinase 1 (Fpk1p) and Fpk2p were recently identified (32). Among the yeast kinases, Fpk1p and Fpk2p exhibit the highest sequence homology to the AGCVIII kinase domain of phototropins (32) (Fig. 1A, supplemental Fig S1). Hence, we reasoned that phototropins might complement the loss of *FPK*s in yeast in a light-dependent manner.

FPK1 and *FPK2* exhibit synthetic growth defects with the null mutation of *CDC50* (36,37). Their products, Fpk1p and Fpk2p, regulate the Lem3p-Dnf1p and Lem3p-Dnf2p flippases, which act as inward-directed phospholipid translocases (38). Nakano et al., have established a conditional mutant in which Cdc50p is expressed under the control of the glucose-repressible *GAL1* promoter in the *fpk1Δ fpk2Δ* background (P_{GAL1}-*CDC50 fpk1Δ fpk2Δ*) (32). The resultant P_{GAL1}-*CDC50 fpk1Δ fpk2Δ* mutant grows normally in galactose-containing medium (SGA-Ura) but exhibits severe growth defect in glucose-containing medium (SDA-Ura) (Fig. 1B) (32).

In order to examine whether phototropins could rescue the loss of *FPKs* in yeast, we introduced the *Arabidopsis PHOT1* (*AtPHOT1*) and *PHOT2* (*AtPHOT2*), and *Chlamydomonas PHOT* (*CrPHOT*) genes into the P_{GAL1}-*CDC50 fpk1Δ fpk2Δ* strain. Consequently, *AtPHOT2* partly suppressed the growth defect in glucose-containing medium regardless of the light condition, whereas *AtPHOT1* completely failed to allow growth (supplemental Fig. S2). Remarkably, *CrPHOT*, albeit partially, suppressed the growth defect under BL but not in darkness (Fig. 1B) or under red light (Fig. 1D). Thus, *Cr*PHOT complemented the loss of Fpk activity in a BL-dependent manner in yeast.

CrPHOT Acts as a Light-Dependent "Flippase-Kinase" in Yeast–We genetically examined whether the kinase activity of *Cr*PHOT was indeed required for the complementation. The kinase domain fragments of phototropins exhibit constitutive kinase activity without light stimulus (17,18). As expected, the kinase domain fragment of *Cr*PHOT restored yeast growth regardless of the light condition (Fig. 1B). Conversely, the D549N mutant of *Cr*PHOT, which corresponded to the kinase-dead mutation in *At*PHOT1 and *At*PHOT2 (17,23), failed to restore growth. The substitution of conserved Cys^{39} to alanine in the LOV2 domain is known to decrease the extent of light activation in phototropins (18,23). The corresponding C250A mutant of *Cr*PHOT restored growth but very weakly (Fig. 1B). Taken together, *Cr*PHOT complemented the loss of Fpks in a kinase-like manner.

We then examined whether the complementation by *Cr*PHOT indeed depended on its light activation.

First, we confirmed that the level of *Cr*PHOT in yeast was not altered under BL with an anti-HA tag antibody (Fig. 1C). This was because phototropin is known to be degraded more rapidly under BL in some cases (7,39). It should be noted that electric mobility shift due to BL-induced autophosphorylation was not observed. This was probably because such activity is low in *Cr*PHOT (11).

We then determined the dependence of complementation by *Cr*PHOT on BL intensity (Fig. 1D). The degree of complementation increased as BL was increased from 0.01 to 10 μmol m^{-2} s^{-1}. This result matched well with those from a previous analysis on the biological activity of *Cr*PHOT expressed in *Arabidopsis* (11).

BL-Dependent Regulation of Phospholipid Uptake by CrPHOT–We further examined whether *Cr*PHOT activated flippases in yeast as Fpks do so. Phosphatidylethanolamine is enriched in the outer leaflet of the membrane in *fpk1Δ fpk2Δ* mutant due to reduced flippase activity. This leads to growth defect in the presence of duramycin, a cytotoxic small tetracyclic peptide that binds phosphatidylethanolamine on the outer leaflet. As expected, *Cr*PHOT rescued the duramycin-sensitive growth defect in a BL-dependent manner (Fig 2). In addition, the kinase fragment rescued the phenotype regardless of the light condition, whereas the putative kinase-dead mutant (D549N) of *Cr*PHOT failed to restore the growth. Hence, *Cr*PHOT was suggested to regulate the flippase activity in yeast.

The Search for Novel CrPHOT Variants Showing Pseudolit Activity–The above experimental system should be potentially useful in identifying amino acid residues important for phototropin functions. To explore this possibility, mutations were separately introduced into the N- and C-terminal moieties of *CrPHOT* by a PCR-based method at the rate of 1.5 mutation/kb (Fig. 3A). Pools of transformed cells corresponding to 5.0×10^5 each of successful recombination events were screened for mutations that allowed growth in darkness on SDA-Ura plates. Consequently, 1504 and 107 growth-positive colonies were obtained for the N- and C-terminal mutant pools, respectively.

We then sequenced 96 randomly selected clones for the N-terminal mutations and all 107 clones for the C-terminal mutations. Consequently, we found that many of them carried multiple amino acid substitutions. In addition, a large deletion, probably due to irregular homologous recombination, was found in some clones. Nonetheless, 8 clones with single amino acid substitutions were identified (Fig. 3A). Additionally, 4 substitutions were shared in more than three independent clones with multiple mutations. Re-introduction of the latter mutations into the wild-type *CrPHOT* confirmed that they indeed conferred the pseudolit phenotype (Fig. 3C, supplemental Fig. S3). We also confirmed that the expression levels of these mutant proteins were not elevated in yeast cells (supplemental Fig. S3).

Kinase Activities of Full-Length CrPHOT Carrying Mutations in the N-terminal Flanking Region of LOV2– Interestingly, 8 out of the above 12 mutations were clustered in a well-conserved N-terminal LOV2 flanking region (residues Arg^{199}-Arg^{210}) (Fig. 3A and B). Hence, their kinase activity was examined *in vitro*. For this purpose, we attempted to express the recombinant full-length *Cr*PHOT protein tagged with an N-terminal 6His tag in *E .coli*. Full-length *Cr*PHOT protein was recovered as a yellow-colored, soluble protein from the *E. coli* extract. For the kinase assay, the *Cr*PHOT protein was purified from the extract by Ni^{2+}-affinity chromatography and size-exclusion chromatography. SDS-PAGE revealed that the resulting sample consisted of a main band of 90 kDa, which corresponded to the theoretical mass of the protein, 85.7 kDa, with several minor bands of lower molecular masses. The purity was then estimated to be approximately 75% (Fig. 4A), which was comparable to those of samples used for the previous kinase assays of LOV-kinase fragments (18,35).

In vitro phosphorylation assay for the purified *Cr*PHOT was performed using the N-terminal fragment of *Arabidopsis* PHOT1 (*At*P1-Nt) as a substrate (35). As expected, *Cr*PHOT phosphorylated *At*P1-Nt under BL, while phosphorylation was substantially reduced in darkness (Fig. 4B). The phosphorylation level increased during the incubation period of 60 min. The effects of BL were saturated at approximately 10 μmol m^{-2} s^{-1} (Fig. 4C). It should be noted that the background activity in darkness was relatively high, which has been reported for other phototropin samples as well (40,41).

We then examined the kinase activities in 6 out of 8 mutants carrying the mutation in the N-terminal flanking region of LOV2 (R199C, D203N, L204P, T207I and R210H). The full-length proteins were expressed in *E. coli* and purified as described above. Consequently, protein samples in similar qualities were obtained with the exception of R199C in which a larger amount of impurity at around 36.5 kDa was detected (Fig. 5A).

We examined the kinase activity using *At*P1-Nt as a substrate. In consistent with the yeast phenotype (Fig. 3), the above mutants exhibited increased kinase activities in darkness compared with the WT with the exception of D203N (Fig. 5*B* and *C*). Hence, most of the *Cr*PHOT mutants disrupted repression of the kinase activity *in vitro*.

Spectroscopic Analysis of the Mutation in the N-terminal Flanking Region of LOV2–We examined whether the present mutations affected the spectral nature of *Cr*PHOT. For this purpose, the T207I mutant was selected as a representative mutant and expressed in *E. coli*. The protein sample conventionally prepared according to the procedure listed for the kinase assay was further purified by negative ion exchange chromatography. Consequently, a sample with > 95% purity was obtained (Fig. 6A).

The absorption spectroscopy revealed that both WT and T207I mutant exhibited the typical fine-structured absorption spectra of protein-bound FMN with absorption maxima at 425, 447 and 472 nm (Fig. 6B). Under continuous BL irradiation, both WT and T207I *Cr*PHOT proteins were converted to cysteinyl adduct state with absorption maxima at 390 nm (Fig. 6B). Those absorption spectra were nearly identical to those of the LOV1-hinge-LOV2 fragment of *Cr*PHOT, which lacked the kinase domain (42).

At a fluence rate of 270 μmol m^{-2} s^{-1}, adduct formation was saturated within 24 s, whereas the dark reversion was completed within 400 s after the illumination was turned off (data not shown). By exponential fitting analysis, the half-lives for dark decay of two photoproduct components in WT *Cr*PHOT were calculated to be 15 and 50 s, whereas those for the T207I mutant were 15 and 56 s. Hence, the T207I mutant was almost indistinguishable from the WT. Taken together, the T207I mutation in the N-terminal flanking region of LOV2 activated the kinase domain without affecting the spectral nature of *Cr*PHOT.

Estimation of Molecular Mass by Size-Exclusion Chromatography–LOV1 domains in phototropins have been suggested to form a dimer (43-45). Hence, we examined the possibility that the T207I mutation affected kinase activity by altering the multimerization state of full-length *Cr*PHOT. To test this possibility, we determined the molecular masses of full-length WT and T207I *Cr*PHOT by size-exclusion chromatography. For this purpose, the samples were purified as for the spectral analysis.

The size-exclusion elution profile demonstrated that both WT and T207I *Cr*PHOT proteins exhibited a major distinct peak at 71.14 ml, corresponding to a molecular mass of 123.7 kDa (supplemental Fig. S5). Hence, the T207I mutation did not alter the multimerization state of full-length *Cr*PHOT. Another minor peak at 78 ml (corresponding to 68 kDa) probably represented a degradation product.

DISCUSSION

CrPHOT Complements the Loss of the Fpk1p and Fpk2p Kinases in Yeast–A bacterial system has been successfully employed to identify amino acid residues important for the spectral integrity of the LOV domains of phototropins (30). The present study further extended this strategy to assess the signaling activity of phototropin derivatives in a microorganism.

Indeed, *Cr*PHOT successfully rescued the *fpk1Δ fpk2Δ* phenotype to allow cell growth in a BL-dependent manner in yeast (Fig. 1). We further demonstrated that both photoexcitation of the LOV domain and the kinase activity of *Cr*PHOT are necessary to promote yeast cell growth (Fig. 1B). Hence, we have developed an experimental system suitable for a large-scale mutant screening for *Cr*PHOT.

It remains unclear why the *Arabiodopsis PHOT1* and *PHOT2* did not function properly in yeast. To gain further insights, the complementation activities of respective kinase fragments were examined. Consequently, the PHOT1 kinase fragment failed to promote the cell growth, whereas the PHOT2 fragment did (supplemental Fig. S2). Hence, intrinsic kinase activities of *Arabiodopsis* PHOT1 and PHOT2 appeared to be quite different in yeast for an unknown reason.

Kinase Activity of Full-Length CrPHOT –It had long been believed that expression of recombinant full-length phototropins in *E. coli* for biochemical analyses was very difficult. Recently however, Pfeifer et al. successfully purified full-length *Cr*PHOT in *E.coli* to conduct FT-IR spectroscopy (46). Similarly, we were able to prepare full-length WT and mutated *Cr*PHOT proteins pure enough for the *in vitro* kinase assay, photochemical kinetic analysis and multimerization analysis.

The BL-dependent kinase activity of the purified *Cr*PHOT was successfully shown *in vitro* using *At*P1-Nt as a substrate (Fig. 4B). As has been shown already for *Cr*PHOT expressed in insect cells (11), autophosphorylation activity was relatively low. This was not because the purified *Cr*PHOT was already phosphorylated in *E. coli* (supplemental Fig.

S6). We suppose fewer phosphorylation sites exist in *Cr*PHOT (11).

Spectral and Multimerization Properties of Full-Length CrPHOT–Fast and slow components observed in the dark decay kinetics (Fig. 6) presumably represented LOV2 and LOV1 ($t_{1/2}$ = 15 and 50 s, respectively). In comparison with the *Cr*PHOT LOV1+LOV2 fragment ($t_{1/2}$ = 17 and 200 s) (47), the slower component was 4 times faster in the full-length *Cr*PHOT. Hence, the presence of the C-terminal kinase domain might alter the photochemical kinetics of LOV1 as previously reported for *Arabidopsis* PHOT1 and PHOT2 (47).

The LOV1 domains of *Arabidopsis* PHOT1 and PHOT2 (43-45) and *Cr*PHOT (48) have been suggested to form a dimer and higher oligomers. However, size-exclusion chromatography in this study hinted that full-length *Cr*PHOT may exist as a monomer (apparent molecular mass of 123.7 kDa vs theoretical mass of 85.7 kDa) (supplemental Fig. S5). This possibility should be further investigated by other methods such as SAXS or crystallization analysis.

Mutations Outside the LOV2 N-terminal Flanking Region– Prior to the present work, several amino acid substitutions in the N-terminal region of phototropins had been known to cause the pseudolit activation. Those include the ones in the Jα helix (V601E, A605E, and I608E in *Arabidopsis* PHOT1) (28) and the LOV2 core region (G513N in *Avena* PHOT1) (49). By contrast, such a mutation had not been known within the C-terminal region. In the present study, 4 novel mutations were found in addition to those clustered in the N-terminal LOV2 flanking region (see below).

Among them, L354P resides in the vicinity of Jα (Fig. 3A, supplemental Fig. S3). This is not surprising because several mutations are already known in this region to cause the pseudolit phenotype (see above). By contrast, Y39C in the LOV1 core region (Fig. 3A, supplemental Fig. S3) was somewhat unexpected because LOV1 is less important than LOV2 to regulate the kinase activity (18,23,24). However, LOV1 modifies the light sensitivity of PHOT2 (18). Hence, this mutation may affect the presumed LOV1/LOV2 or LOV1/kinase interaction to substantially increase the light sensitivity.

The N610S/T mutations in the activation loop of the kinase domain conferred the pseudolit phenotype (Fig. 3A, supplemental Fig. S3). Interestingly, the Asn^{610} residue is adjacent to Ser^{611}, which corresponds to the autophosphorylation site required for the activation of both PHOT1 and PHOT2 in *Arabidopsis* (13,14) (supplemental Fig. S1). We constructed the N610A *Cr*PHOT to show that Ser^{610} and Thr^{610} but not Ala^{610} caused the pseudolit activation (supplemental Fig. S3). Hence, the newly introduced Ser/Thr^{610} might have acted as a secondary phosphorylation site to increase the kinase activity.

Involvement of the N-terminal Flanking Region of LOV2 in Light-Induced Signal Transduction–In our screening, we identified a novel mutational hot spot in the N-terminal flanking region of LOV2 (Arg^{199}-Arg^{210} in Fig. 3A). These mutations substantially reduced repression of the kinase activity by the N-terminal moiety in darkness (Figs. 3, 5) without affecting the photochemical (Fig. 6) or multimerization properties of *Cr*PHOT (Supplemental Fig. S6).

The crystal structure of LOV2 with N- and C-terminal flanking regions from *Avena* PHOT1 (residues Leu^{404}-Ala^{559} in *Avena* PHOT1) indicates that the N-terminal region (residues Leu^{404}-Arg^{414} in *Avena* PHOT1) is in the turn-helix-turn structure, in which the helix has been denoted as A'α (residues Thr^{407}-Arg^{410} in *Avena* PHOT1) (22). In this structure, A'α is packed against the surface of the β-sheet of the LOV2 core domain to interact with the Jα helix (residues Asp^{522}-Ala^{543} in *Avena* PHOT1) in the C-terminal flanking region. Importantly, the light-induced structural rearrangements within the LOV2 core are associated with displacement of residues surrounding A'α (22). Hence, not only the C-terminal Jα helix but also the N-terminal flanking region are proposed to act as interfaces relaying the signal from the LOV2 core to the outside domain.

Our mutational analysis shed new light on the biochemical function of the N-terminal flaking region of LOV2. The sequences in this region (Arg^{199}-Arg^{210}) are strikingly conserved among different phototropins (Fig. 3B). The alignment suggests that T207I and R210H reside within A'α whereas L204P is in the loop upstream of A'α. Although the other three mutational sites, R199C, L202P and D203N/G/V, are excluded from the above structural study, they are in close proximity on the primary structure. It should be noted here that a high degree of homology does not warrant similar phenotype in corresponding mutants of other phototropins. Indeed, *Arabidopsis* PHOT1 carrying T469I (corresponding to T207I in *Cr*PHOT) failed to show pseudolit activation (data not shown).

The Hypothetical Extended A'α Helix May Play an Important Role for Intramolecular

Signaling–Interestingly, a secondary-structure prediction suggests that the A'α helix could be extended towards the N-terminus to form a longer α helix (Arg^{199}-Arg^{210}), within which all the 6 mutational sites are mapped (supplemental Fig. S7A). Furthermore, the presumed α helix shows amphipathic character (supplemental Fig. S7B). The hydrophobic surface of this helix might then be packed against the hydrophobic LOV2 core. If this prediction is correct, the mutated residues residing in the polar surface of the helix (Arg^{199}, Asp^{203}, Thr^{207}, and Arg^{210}) might be directly involved in the physical interaction with other functional domains, such as the Jα-helix and the C-terminal kinase. The existence of and a structural role for the predicted helix must be investigated in future studies.

REFERENCE

1. Christie, J. M. (2007) *Annu Rev Plant Biol* **58**, 21-45
2. Huala, E., Oeller, P. W., Liscum, E., Han, I. S., Larsen, E., and Briggs, W. R. (1997) *Science* **278**, 2120-2123
3. Sakai, T., Kagawa, T., Kasahara, M., Swartz, T. E., Christie, J. M., Briggs, W. R., Wada, M., and Okada, K. (2001) *Proc Natl Acad Sci U S A* **98**, 6969-6974
4. Jarillo, J. A., Gabrys, H., Capel, J., Alonso, J. M., Ecker, J. R., and Cashmore, A. R. (2001) *Nature* **410**, 952-954
5. Kagawa, T., Sakai, T., Suetsugu, N., Oikawa, K., Ishiguro, S., Kato, T., Tabata, S., Okada, K., and Wada, M. (2001) *Science* **291**, 2138-2141
6. Kinoshita, T., Doi, M., Suetsugu, N., Kagawa, T., Wada, M., and Shimazaki, K. (2001) *Nature* **414**, 656-660
7. Sakamoto, K., and Briggs, W. R. (2002) *Plant Cell* **14**, 1723-1735
8. Kozuka, T., Kong, S. G., Doi, M., Shimazaki, K. I., and Nagatani, A. (2011) *Plant Cell*
9. Huang, K., and Beck, C. F. (2003) *Proc Natl Acad Sci U S A* **100**, 6269-6274
10. Im, C. S., Eberhard, S., Huang, K., Beck, C. F., and Grossman, A. R. (2006) *Plant J* **48**, 1-16
11. Onodera, A., Kong, S. G., Doi, M., Shimazaki, K., Christie, J., Mochizuki, N., and Nagatani, A. (2005) *Plant Cell Physiol* **46**, 367-374
12. Galvan-Ampudia, C. S., and Offringa, R. (2007) *Trends Plant Sci* **12**, 541-547
13. Inoue, S., Kinoshita, T., Matsumoto, M., Nakayama, K. I., Doi, M., and Shimazaki, K. (2008) *Proc Natl Acad Sci U S A* **105**, 5626-5631
14. Inoue, S., Matsushita, T., Tomokiyo, Y., Matsumoto, M., Nakayama, K. I., Kinoshita, T., and Shimazaki, K. (2011) *Plant Physiol* **156**, 117-128
15. Christie, J. M., Yang, H., Richter, G. L., Sullivan, S., Thomson, C. E., Lin, J., Titapiwatanakun, B., Ennis, M., Kaiserli, E., Lee, O. R., Adamec, J., Peer, W. A., and Murphy, A. S. (2011) *PLoS Biol* **9**, e1001076
16. Crosson, S., and Moffat, K. (2001) *Proc Natl Acad Sci U S A* **98**, 2995-3000
17. Kong, S. G., Kinoshita, T., Shimazaki, K., Mochizuki, N., Suzuki, T., and Nagatani, A. (2007) *Plant J* **51**, 862-873

18. Matsuoka, D., and Tokutomi, S. (2005) *Proc Natl Acad Sci U S A* **102**, 13337-13342
19. Salomon, M., Christie, J. M., Knieb, E., Lempert, U., and Briggs, W. R. (2000) *Biochemistry* **39**, 9401-9410
20. Swartz, T. E., Corchnoy, S. B., Christie, J. M., Lewis, J. W., Szundi, I., Briggs, W. R., and Bogomolni, R. A. (2001) *J Biol Chem* **276**, 36493-36500
21. Crosson, S., and Moffat, K. (2002) *Plant Cell* **14**, 1067-1075
22. Halavaty, A. S., and Moffat, K. (2007) *Biochemistry* **46**, 14001-14009
23. Christie, J. M., Swartz, T. E., Bogomolni, R. A., and Briggs, W. R. (2002) *Plant J* **32**, 205-219
24. Cho, H. Y., Tseng, T. S., Kaiserli, E., Sullivan, S., Christie, J. M., and Briggs, W. R. (2007) *Plant Physiol* **143**, 517-529
25. Harper, S. M., Neil, L. C., and Gardner, K. H. (2003) *Science* **301**, 1541-1544
26. Chen, E., Swartz, T. E., Bogomolni, R. A., and Kliger, D. S. (2007) *Biochemistry* **46**, 4619-4624
27. Yamamoto, A., Iwata, T., Sato, Y., Matsuoka, D., Tokutomi, S., and Kandori, H. (2009) *Biophys J* **96**, 2771-2778
28. Harper, S. M., Christie, J. M., and Gardner, K. H. (2004) *Biochemistry* **43**, 16184-16192
29. Takayama, Y., Nakasako, M., Okajima, K., Iwata, A., Kashojiya, S., Matsui, Y., and Tokutomi, S. (2011) *Biochemistry* **50**, 1174-1183
30. Christie, J. M., Corchnoy, S. B., Swartz, T. E., Hokenson, M., Han, I. S., Briggs, W. R., and Bogomolni, R. A. (2007) *Biochemistry* **46**, 9310-9319
31. Rose, M. D., Winston, F., and Hieter, P. (1990) *A Laboratory Course Manual, Cold Spring Harbor, NY: Cold Spring Horbor Laboratory Press*
32. Nakano, K., Yamamoto, T., Kishimoto, T., Noji, T., and Tanaka, K. (2008) *Mol Biol Cell* **19**, 1783-1797
33. Sikorski, R. S., and Hieter, P. (1989) *Genetics* **122**, 19-27
34. Kushnirov, V. V. (2000) *Yeast* **16**, 857-860
35. Okajima, K., Matsuoka, D., and Tokutomi, S. (2011) *FEBS Lett* **585**, 3391-3395
36. Saito, K., Fujimura-Kamada, K., Furuta, N., Kato, U., Umeda, M., and Tanaka, K. (2004) *Mol Biol Cell* **15**, 3418-3432
37. Chen, S., Wang, J., Muthusamy, B. P., Liu, K., Zare, S., Andersen, R. J., and Graham, T. R. (2006) *Traffic* **7**, 1503-1517
38. Pomorski, T., Lombardi, R., Riezman, H., Devaux, P. F., van Meer, G., and Holthuis, J. C. (2003) *Mol Biol Cell* **14**, 1240-1254
39. Kong, S. G., Suzuki, T., Tamura, K., Mochizuki, N., Hara-Nishimura, I., and Nagatani, A. (2006) *Plant J* **45**, 994-1005
40. Jones, M. A., and Christie, J. M. (2008) *Plant Signal Behav* **3**, 44-46
41. Jones, M. A., Feeney, K. A., Kelly, S. M., and Christie, J. M. (2007) *J Biol*

Chem **282**, 6405-6414
42. Guo, H., Kottke, T., Hegemann, P., and Dick, B. (2005) *Biophys J* **89**, 402-412
43. Nakasako, M., Iwata, T., Matsuoka, D., and Tokutomi, S. (2004) *Biochemistry* **43**, 14881-14890
44. Salomon, M., Lempert, U., and Rudiger, W. (2004) *FEBS Lett* **572**, 8-10
45. Nakasako, M., Zikihara, K., Matsuoka, D., Katsura, H., and Tokutomi, S. (2008) *J Mol Biol* **381**, 718-733
46. Pfeifer, A., Mathes, T., Lu, Y., Hegemann, P., and Kottke, T. (2010) *Biochemistry* **49**, 1024-1032
47. Kasahara, M., Swartz, T. E., Olney, M. A., Onodera, A., Mochizuki, N., Fukuzawa, H., Asamizu, E., Tabata, S., Kanegae, H., Takano, M., Christie, J. M., Nagatani, A., and Briggs, W. R. (2002) *Plant Physiol* **129**, 762-773
48. Kutta, R. J., Hofinger, E. S., Preuss, H., Bernhardt, G., and Dick, B. (2008) *Chembiochem* **9**, 1931-1938
49. Nash, A. I., Ko, W. H., Harper, S. M., and Gardner, K. H. (2008) *Biochemistry* **47**, 13842-13849

Acknowledgements - We thank Prof. Masato Umeda and Dr. Utako Kato from Kyoto university for helpful discussion.

FOOT NOTES

*This work was supported by; a Grant-in-Aid for Scientific Research on Priority Areas (No. 17084002 to A.N.), a Grant-in-Aid for Scientific Research on Innovative Areas (No. 22120002 to A.N.) and a Grant-in-Aid for the Global COE Program 'Formation of a strategic base for biodiversity and evolutionary research: from genome to ecosystem' (to A.N.), from Ministry of Education, Culture, Sports, Science and Technology, Japan; and a Grant-in-Aid for Scientific Research (B) (No. 21370020 to A.N.) and a research fellowship (No. 22.1094 to Y.A.) from the Japan Society for the Promotion of Science.
To whom correspondence should be addressed: Akira Nagatani, Tel.: +81 75-753-4123; fax: +81 75-753-4126; e-mail: nagatani@physiol.bot.kyoto-u.ac.jp.
The abbreviations used are: PHOT, phototropin; BL, blue light; LOV, Light-Oxygen and Voltage; PAS, Per-ARNT-Sim; FMN, flavin mononucleotide; *Cr*PHOT, *Chlamydomonas* phototropin; *Escherichia* col, *E. coli*; HA, influenza virus hemagglutinin epitope; *At*P1-Nt; N-terminal fragment of *Arabidopsis* PHOT1; CBB, Coomassie brilliant blue; Fpk1p, flippase-kinase 1.

FIGURE LEGENDS

FIGURE 1. Photoregulation of yeast cell-growth by *Cr*PHOT. The yeast conditional mutant P_{GAL1}-*CDC50 fpk1*Δ *fpk2*Δ was transformed with a vector containing the *FPK1* gene or *CrPHOT* derivatives fused to the constitutive *TPI1* promoter. A, Schematic illustration of the phototropin from *Chlamydomonas reinhardtii* (*Cr*PHOT) and Fpk1p and Fpk2p from *Saccharomyces cerevisiae*. The numbers within the Ser/Thr kinase domain show the percentage sequence identity with the *Cr*PHOT kinase domain. B, Growth of the yeast conditional mutant P_{GAL1}-*CDC50 fpk1*Δ *fpk2*Δ expressing the full-length *CrPHOT* and its derivatives. Yeast cells were serially diluted and spotted

onto plates containing galactose (SGA-Ura) or glucose (SDA-Ura), followed by incubation in darkness (Dark) or under BL irradiation (50 μmol m^{-2} s^{-1} ; Blue) at 28°C for 2-3 d. Empty, yeast cells transformed with a control plasmid. C, Immunoblot detection of the full-length *Cr*PHOT with an anti-HA monoclonal antibody in yeast grown as for B. Protein extracts from 1 mg of wet yeast cells were separated by 10.0% SDS-PAGE. D, Effects of monochromatic light irradiation on growth of yeast expressing *CrPHOT*. Red light at 50 μmol m^{-2} s^{-1} or blue light at different intensities were applied to yeast cells as for B.

FIGURE 2. Growth sensitivity to duramycin of the *fpk1*Δ *fpk2*Δ mutant expressing *CrPHOT* and its derivatives. The yeast cells were serially diluted and spotted onto YPDA plates with or without 10 μM duramycin. The plates were then incubated in darkness (Dark) or under BL irradiation (50 μmol m^{-2} s^{-1} ; Blue) at 28°C for 1.5 d.

FIGURE 3. The *CrPHOT* mutants that restored yeast growth in darkness. A, A schematic drawing of the domain structure of *Cr*PHOT and locations of amino acid substitutions found in the present studies. Gray closed circles indicate mutations identified in clones with a single mutation. Open circles indicate mutations found in more than 3 independent clones with multiple mutations. B, Sequence alignment of N-terminal flanking regions of LOV2 among different phototropin species. *Cr*_PHOT, *Chlamydomonas reinhardtii* phot; *At*_PHOT1, *Arabidopsis thaliana* PHOT1; *As*_PHOT1; *Avena sativ*a PHOT1; and *At*_PHOT2, *Arabidopsis thaliana* PHOT2. Sequences were aligned using the CLUSTAL W and BOXSHADE program. C, Growth of the P_{GAL1}-*CDC50 fpk1*Δ *fpk2*Δ mutant expressing *CrPHOT* with single amino-acid substitutions. Cells were treated as for Fig. 1B. Two concentrations of yeast cells (a: A_{600} = 0.004, b: A_{600} = 0.0008) were spotted.

FIGURE 4. *In vitro* phosphorylation assay of the full-length *Cr*PHOT. A, 10.0% SDS-PAGE gel pattern of full-length *Cr*PHOT stained with CBB. The sample with an N-terminal 6His tag was successively purified by Ni^{2+}-ion affinity chromatography and size-exclusion chromatography. The triangle indicates the position of the intact *Cr*PHOT. B, *In vitro* phosphorylation assay for *Cr*PHOT under BL (100 μmol m^{-2} s^{-1}) or in the dark. *Cr*PHOT and/or *At*P1-Nt were incubated with radioactive ATP for the indicated durations. The upper and lower panels show the 10.0% SDS-PAGE gel patterns visualized by autoradiography and CBB staining, respectively. (+) or (-), the presence or absence of the kinase and/or the substrate, respectively; D, dark condition; L, BL irradiation. C, Dependence of the kinase activation on the light intensity. *In vitro* phosphorylation assay of *Cr*PHOT was performed as described for B. The samples were incubated for 10 min under BL at the indicated light intensities. Phosphorylated *At*P1-Nt was visualized by autoradiography.

FIGURE 5. Effects of *Cr*PHOT mutations on *in vitro* phosphorylation activity. A, 10.0% SDS-PAGE gel patterns of the mutant *Cr*PHOT proteins stained with CBB. The wild-type (WT) and the mutant *Cr*PHOT proteins were prepared as for Figure 4A. The triangle indicates the position of the intact *Cr*PHOT. B, *In vitro* phosphorylation assay for the WT and mutant *Cr*PHOT samples. The reaction proceeded for 30 min under BL (100 μmol m^{-2} s^{-1}) or in the dark condition. Sample preparation and experimental procedures were the same as those for Figure 4B. The upper and lower panels show the 10.0% SDS-PAGE gel patterns visualized by autoradiography and CBB staining, respectively. C, Quantification of the phosphorylation activity in the WT and the mutant *Cr*PHOT. An *in vitro* phosphorylation assay was performed as for B. Band intensities were quantified by a bioimaging analyzer and expressed relative to the maximal phosphorylation level in the WT under BL. The data represent the means of 3 independent experiments. Error bars, standard deviations.

FIGURE 6. Effects of the T207 mutation on photochemical properties. A, 10.0% SDS-PAGE gel pattern of full-length *Cr*PHOT samples stained with CBB. The sample was prepared using the same procedures as those for Figure 5 and was further purified by anion-change chromatography. The triangle indicates the position of the intact *Cr*PHOT. B, Absorption spectra of the WT and the T207I mutant *Cr*PHOT in darkness (solid black lines) and under BL irradiation at 50 μmol m^{-2} s^{-1} (dashed

black lines) and 270 μmol m^{-2} s^{-1} (gray lines). The data represent the means of 3 measurements. C, Kinetics of the reversion of the cysteinyl adduct state to the dark state monitored by the absorption at 450 nm. The samples were equilibrated under BL at 270 μmol m^{-2} s^{-1}, and the light was then tuned off at time 0. The remaining photo adduct level was calculated as $1-(A_t-A_0)/(A_\infty-A_0)$, where A_t, A_∞ and A_0 are absorptions at 450 nm at time t in second, in darkness and under BL, respectively. The logarithm of the remaining photo adduct level was plotted against t in the inset, indicating the fast and slow components of the reversion kinetics.

Figure 1

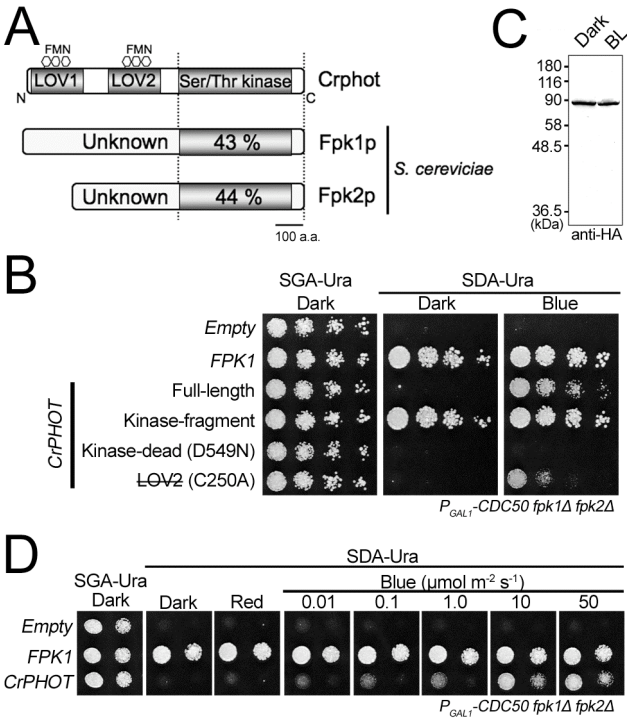
A
FMN
FMN
LOV1
LOV2
Ser/Thr kinase
Crphot
N
C
Unknown
43 %
Fpk1p
Unknown
44 %
Fpk2p
S. cereviciae
100 a.a.
C
Dark
BL
180
116
90
58
48.5
36.5
(kDa)
anti-HA
B
SGA-Ura
Dark
SDA-Ura
Dark
Blue
Empty
FPK1
Full-length
Kinase-fragment
Kinase-dead (D549N)
~~LOV2~~ (C250A)
CrPHOT
P GAL1-CDC50 fpk1Δ fpk2Δ
D
SDA-Ura
SGA-Ura
Dark
Blue (μmol m-2 s-1)
Dark
Red
0.01
0.1
1.0
10
50
Empty
FPK1
CrPHOT
P GAL1-CDC50 fpk1Δ fpk2Δ

Figure 2

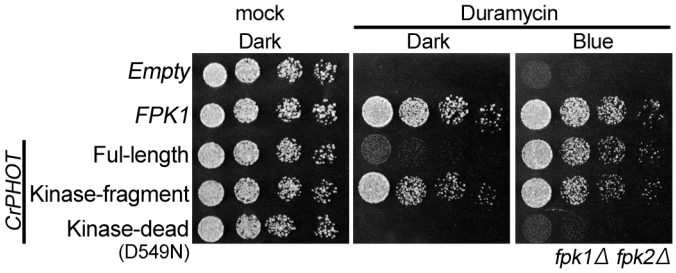
mock
Duramycin
Dark
Dark
Blue
Empty
FPK1
Ful-length
Kinase-fragment
Kinase-dead
(D549N)
CrPHOT
fpk1Δ fpk2Δ

Figure 3

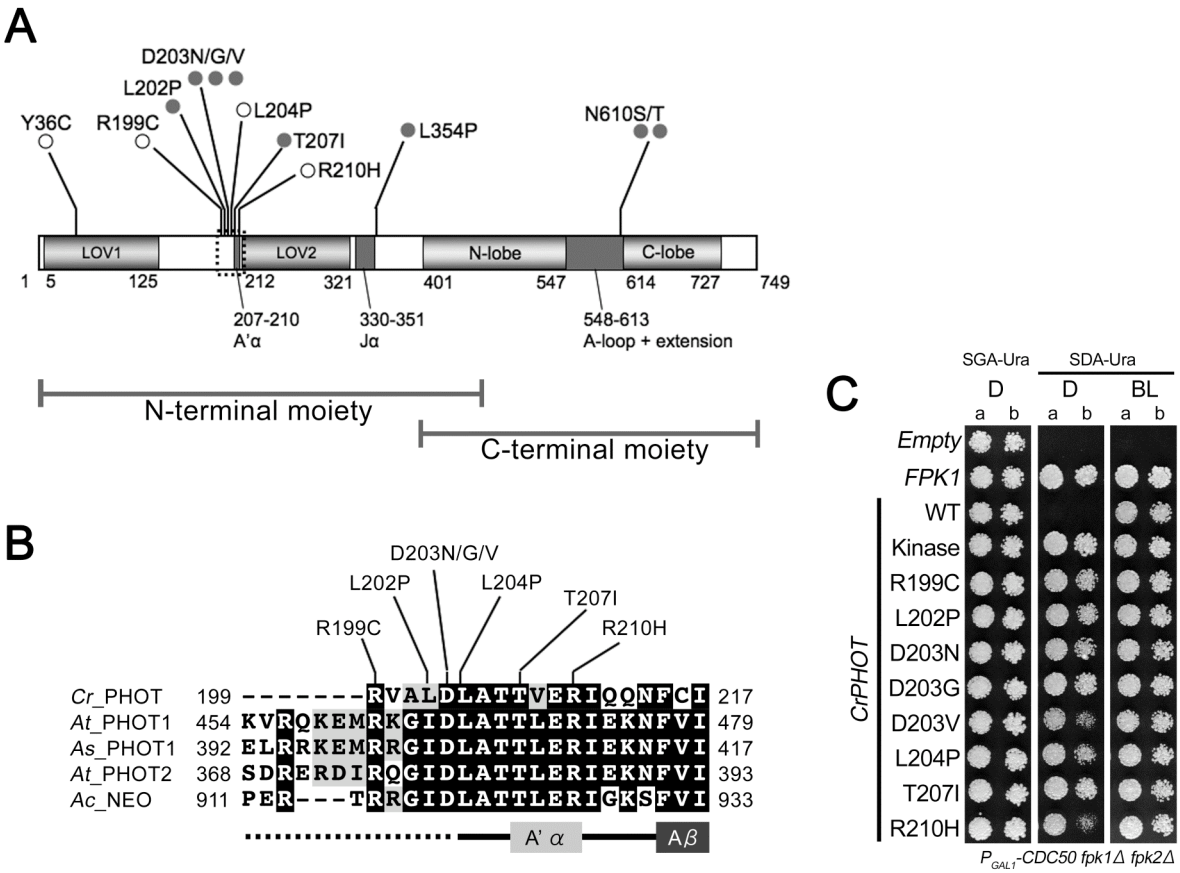
A
D203N/G/V
L202P
L204P
Y36C
R199C
T207I
L354P
R210H
N610S/T
LOV1
LOV2
N-lobe
C-lobe
1 5 125 212 321 401 547 614 727 749
207-210
A'α
330-351
Jα
548-613
A-loop + extension
N-terminal moiety
C-terminal moiety
B
D203N/G/V
L202P
L204P
T207I
R199C
R210H
Cr_PHOT 199 -------RVALDLATTVERIQQNFCI 217
At_PHOT1 454 KVRQKEMRKGIDLATTLERIEKNFVI 479
As_PHOT1 392 ELRRKEMRRGIDLATTLERIEKNFVI 417
At_PHOT2 368 SDRERDIRQGIDLATTLERIEKNFVI 393
Ac_NEO 911 PER---TRRGIDLATTLERIGKSFVI 933
A' α
Aβ
C
SGA-Ura
SDA-Ura
D
D
BL
a b a b a b
Empty
FPK1
WT
Kinase
R199C
L202P
D203N
D203G
D203V
L204P
T207I
R210H
CrPHOT
P GAL1 -CDC50 fpk1Δ fpk2Δ

Figure 4

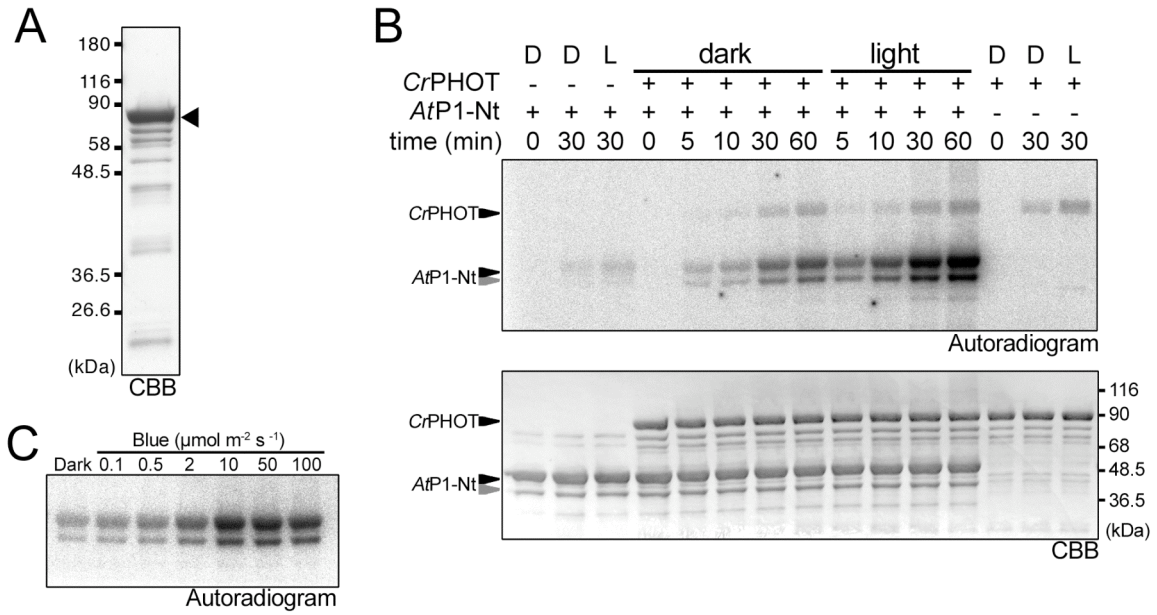
A
180
116
90
58
48.5
36.5
26.6
(kDa)
CBB
B
D D L dark light D D L
CrPHOT - - - + + + + + + + + + + + +
AtP1-Nt + + + + + + + + + + + + - - -
time (min) 0 30 30 0 5 10 30 60 5 10 30 60 0 30 30
CrPHOT
AtP1-Nt
Autoradiogram
CrPHOT
AtP1-Nt
116
90
68
48.5
36.5
(kDa)
CBB
C
Blue (μmol m-2 s -1)
Dark 0.1 0.5 2 10 50 100
Autoradiogram

Figure 5

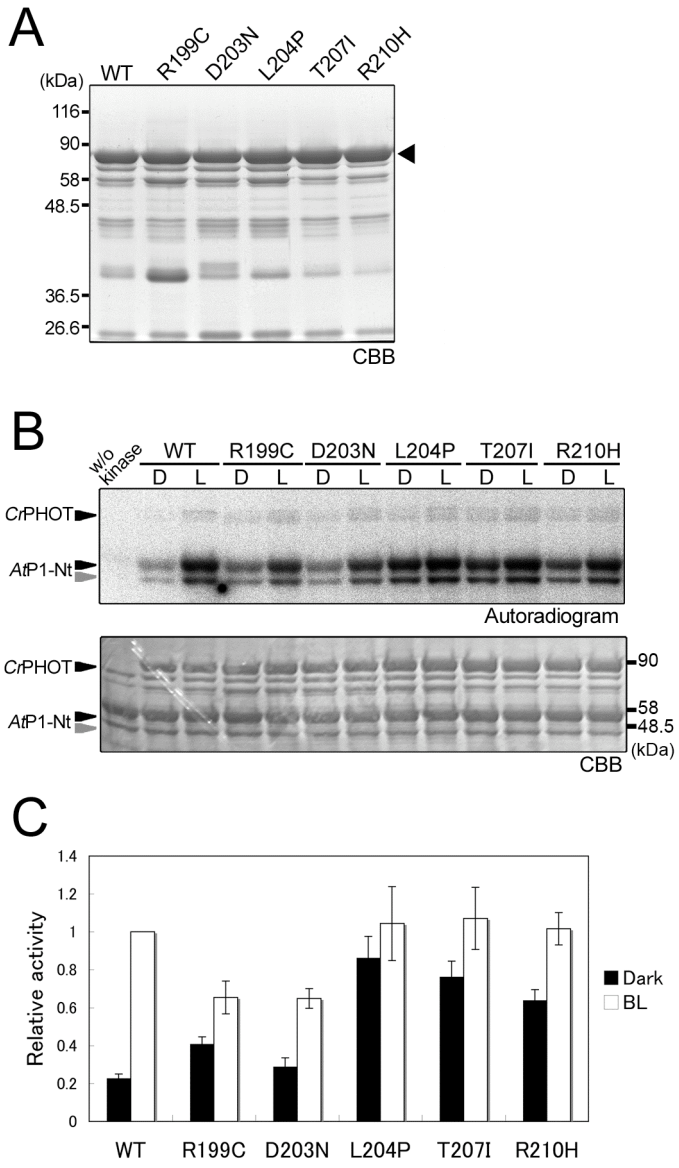
A
(kDa)
WT
R199C
D203N
L204P
T207I
R210H
116
90
58
48.5
36.5
26.6
CBB
B
w/o kinase
WT
R199C
D203N
L204P
T207I
R210H
D L D L D L D L D L D L
CrPHOT
AtP1-Nt
Autoradiogram
CrPHOT
AtP1-Nt
90
58
48.5
(kDa)
CBB
C
Relative activity
1.4
1.2
1
0.8
0.6
0.4
0.2
0
Dark
BL
WT
R199C
D203N
L204P
T207I
R210H

Figure 6

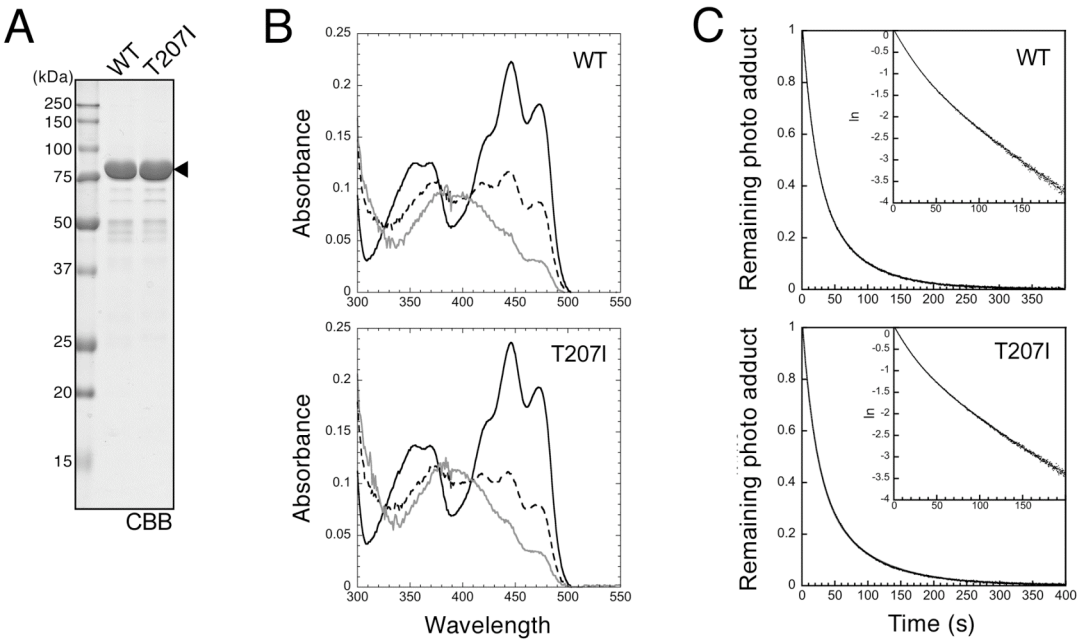
A
WT
T207I
(kDa)
250
150
100
75
50
37
25
20
15
CBB
B
WT
T207I
Absorbance
Wavelength
C
WT
T207I
Remaining photo adduct
ln
Time (s)

Aihara et al., 2011

SUPPLEMENTAL FIGURES

Figure S1. Comparison of the amino acid sequences of the kinase domains of Fpk1p, Fpk2p and *Cr*PHOT. The sequences were aligned using the CLUSTAL W and BOXSHADE program. Regions of the N-terminal lobe, the activation loop plus extension and the C-terminal lobe are indicated by the blue, green and red lines respectively. Black triangle, the serine residue for which autophosphorylation is required for the activation of both phot1 and phot2 in *Arabidopsis* (12, 13).

Figure S2. P_{GAL1}-*CDC50 fpk1*Δ *fpk2*Δ cell growth in the presence of *Arabidopsis* PHOT1 and PHOT2. The yeast mutant was transformed with a vector containing *FPK1, AtPHOT1, AtPHOT2* and the kinase domains of *AtPHOT1* and *AtPHOT2* fused to the constitutive *TPI1* promoter. Yeast cells were serially diluted, spotted onto plates containing galactose (SGA-Ura) or glucose (SDA-Ura), and incubated in darkness (Dark) or under BL irradiation (50 μmol m^{-2} s^{-1} ; Blue) at 28°C for 2-3 d.

Figure S3. Growth of the P_{GAL1}-*CDC50 fpk1*Δ *fpk2*Δ mutant expressing *CrPHOT* with single amino-acid substitutions other than those within the N-terminal flanking region of LOV2. Cells were treated with light as for Figure S2. Two concentrations of yeast cells (a: A_{600} = 0.004, b: A_{600} = 0.0008) were spotted.

Figure S4. Immunoblot detection of *Cr*PHOT in the P_{GAL1}-*CDC50 fpk1*Δ *fpk2*Δ yeast cells expressing *CrPHOT* mutants. Protein extracts from 1 mg of wet yeast cells were separated by 10.0 % SDS-PAGE and probed with an anti-HA monoclonal antibody. The cells were grown on SGA-Ura plates at 28°C for 3 d in darkness (D) or under BL at 50 μmol m^{-2} s^{-1} (L) before harvest.

Figure S5. Estimation of the molecular weight of the WT (black line) and the T207I mutant *Cr*PHOT (gray dashed line) by size-exclusion column chromatography. Elution profiles from the Superdex 200 pg hiload column were obtained for the samples purified using the same procedures as those for Figure 6 at 0-4°C under dim red light. The peak positions of the standard proteins used for calibration are indicated by arrowheads. The peak heights were set to 1 to normalize the profiles.

Figure S6. Staining of the phosphorylated *Cr*PHOT purified from *E. coli*. *Cr*PHOT and *At*P1-Nt was purified as for Figure 4 and incubated with or without λ protein phosphatase (λ-PPase) for 1 hr at 37°C. The left and right panels show the 10.0% SDS-PAGE gel electrophoretic patterns visualized by Pro-Q Diamond and CBB staining, respectively.

Figure S7. The hypothetical "extended A'α helix". A, Secondary-structure prediction for the *Cr*PHOT LOV2 domain was performed using the PSIPRED Protein Structure Prediction Server available at http://bioinf.cs.ucl.ac.uk/psipred/. Confidence of the prediction is shown above the secondary structural elements. Regions of the hypothetical extended A'α helix, the LOV2 core and the hypothetical Jα helix are indicated by the blue, green and red boxes, respectively. B, A helical wheel of the hypothetical extended A'α helix of the *Cr*PHOT LOV2 domain (Arg^{199}-Arg^{210}). Red, positively charged; blue, negative charged; green, uncharged but hydrophilic; black, hydrophobic. The polar side of the helix is marked with a black arc. The helical wheel analysis was performed using the pepwheel program (http://inn-temp.weizmann.ac.il/cgi-bin/emboss/pepwheel). Amino acid substitutions identified in this study are denoted in italic letters.

Figure S1

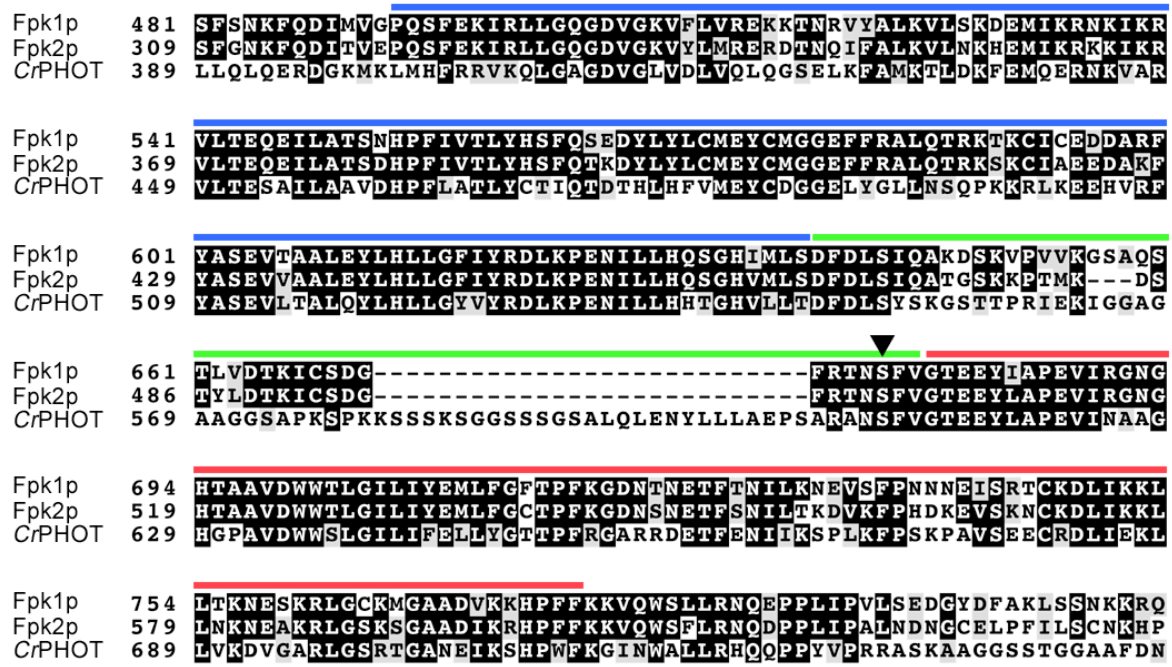
Fpk1p 481 SFSNKFQDIMVGPQSFEKIRLLGQGDVGKVFLVREKKTNRVYALKVLSKDEMIKRNKIKR
Fpk2p 309 SFGNKFQDITVEPQSFEKIRLLGQGDVGKVYLMRERDTNQIFALKVLNKHEMIKRKKIKR
CrPHOT 389 LLQLQERDGKMKLMHFRRVKQLGAGDVGLVDLVQLQGSELKFAMKTLDKFEMQERNKVAR
Fpk1p 541 VLTEQEILATSNHPFIVTLYHSFQSEDYLYLCMEYCMGGEFFRALQTRKTKCICEDDARF
Fpk2p 369 VLTEQEILATSDHPFIVTLYHSFQTKDYLYLCMEYCMGGEFFRALQTRKSKCIAEEDAKF
CrPHOT 449 VLTESAILAAVDHPFLATLYCTIQTDTHLHFVMEYCDGGELYGLLNSQPKKRLKEEHVRF
Fpk1p 601 YASEVTAALEYLHLLGFIYRDLKPENILLHQSGHIMLSDFDLSIQAKDSKVPVVKGSAQS
Fpk2p 429 YASEVVAALEYLHLLGFIYRDLKPENILLHQSGHVMLSDFDLSIQATGSKKPTMK---DS
CrPHOT 509 YASEVLTALQYLHLLGYVYRDLKPENILLHHTGHVLLTDFDLSYSKGSTTPRIEKIGGAG
Fpk1p 661 TLVDTKICSDG----------FRTNSFVGTEEYIAPEVIRGNG
Fpk2p 486 TYLDTKICSDG----------FRTNSFVGTEEYLAPEVIRGNG
CrPHOT 569 AAGGSAPKSPKKSSSKSGGSSSGSALQLENYLLLAEPSARANSFVGTEEYLAPEVINAAG
Fpk1p 694 HTAAVDWWTLGILIYEMLFGFTPFKGDNTNETFTNILKNEVSFPNNNEISRTCKDLIKKL
Fpk2p 519 HTAAVDWWTLGILIYEMLFGCTPFKGDNSNETFSNILTKDVKFPHDKEVSKNCKDLIKKL
CrPHOT 629 HGPAVDWWSLGILIFELLYGTTPFRGARRDETFENIIKSPLKFPSKPAVSEECRDLIEKL
Fpk1p 754 LTKNESKRLGCKMGAADVKKHPFFKKVQWSLLRNQEPPLIPVLSEDGYDFAKLSSNKKRQ
Fpk2p 579 LNKNEAKRLGSKSGAADIKRHPFFKKVQWSFLRNQDPPLIPALNDNGCELPFILSCNKHP
CrPHOT 689 LVKDVGARLGSRTGANEIKSHPWFKGINWALLRHQQPPYVPRRASKAAGGSSTGGAAFDN

Figure S2

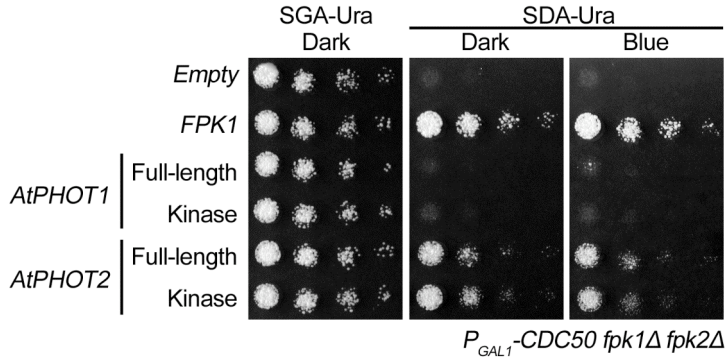
SGA-Ura
Dark
SDA-Ura
Dark
Blue
Empty
FPK1
AtPHOT1
Full-length
Kinase
AtPHOT2
Full-length
Kinase
P GAL1 -CDC50 fpk1Δ fpk2Δ

Figure S3

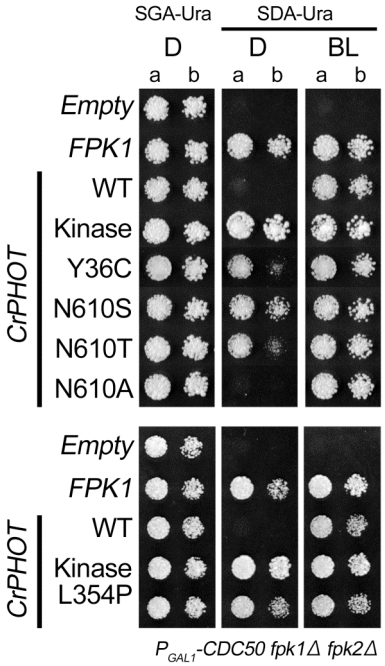
SGA-Ura
SDA-Ura
D
D
BL
a b a b a b
Empty
FPK1
WT
Kinase
Y36C
N610S
N610T
N610A
CrPHOT
Empty
FPK1
WT
Kinase L354P
CrPHOT
P GAL1-CDC50 fpk1Δ fpk2Δ

Figure S4

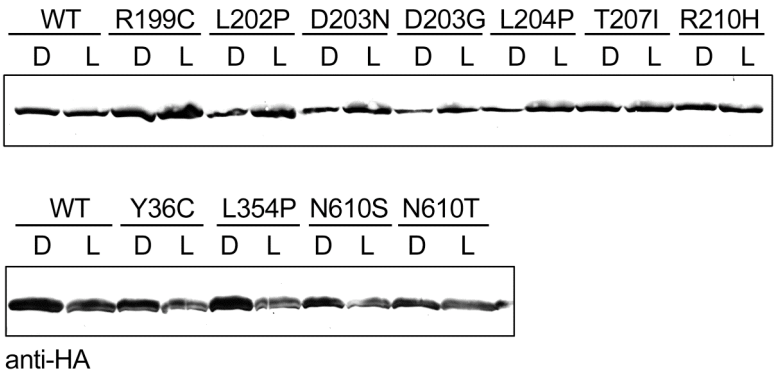
WT
R199C
L202P
D203N
D203G
L204P
T207I
R210H
D L D L D L D L D L D L D L D L
WT
Y36C
L354P
N610S
N610T
D L D L D L D L D L
anti-HA

Figure S5

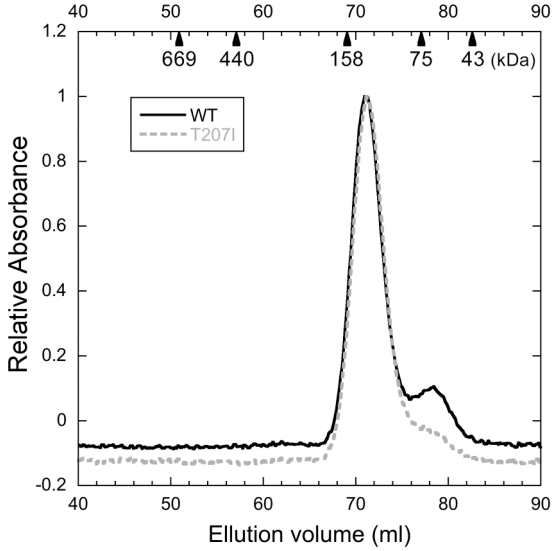
669
440
158
75
43 (kDa)
WT
T207I
Relative Absorbance
Ellution volume (ml)

Figure S6

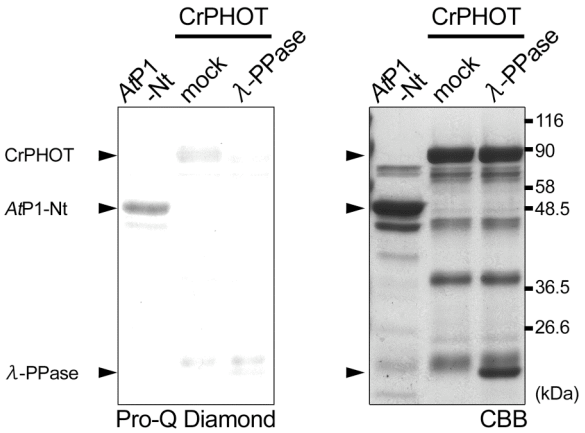
CrPHOT
AtP1 -Nt
mock
λ-PPase
CrPHOT
AtP1-Nt
λ-PPase
Pro-Q Diamond
CrPHOT
AtP1 -Nt
mock
λ-PPase
116
90
58
48.5
36.5
26.6
(kDa)
CBB

Figure S7

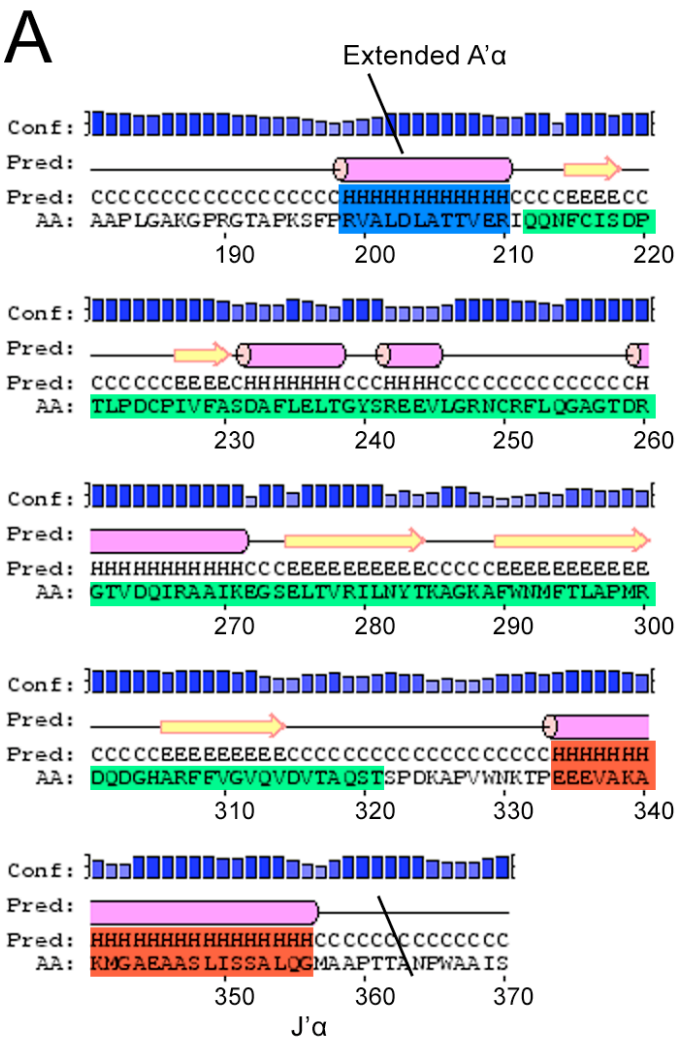
A
Extended A'α
Conf:
Pred:
Pred: CCCCCCCCCCCCCCCCCCHHHHHHHHHHHHCCCCEEEECC
AA: AAPLGAKGPRGTAPKSFPRVALDLATTVERIQQNFCISDP
190
200
210
220
Conf:
Pred:
Pred: CCCCCCEEEECHHHHHHHCCCHHHHCCCCCCCCCCCCCH
AA: TLPDCPIVFASDAFLELTGYSREEVLGRNCRFLQGAGTDR
230
240
250
260
Conf:
Pred:
Pred: HHHHHHHHHHHCCCEEEEEEEEEECCCCCEEEEEEEEEE
AA: GTVDQIRAAIKEGSELTVRILNYTKAGKAFWNMFTLAPMR
270
280
290
300
Conf:
Pred:
Pred: CCCCCEEEEEEEEECCCCCCCCCCCCCCCCCCHHHHHHH
AA: DQDGHARFFVGVQVDVTAQSTSPDKAPVWNKTPEEEVAKA
310
320
330
340
Conf:
Pred:
Pred: HHHHHHHHHHHHHHHHCCCCCCCCCCCCCC
AA: KMGAEAASLISSALQGMAAPTTANPWAAIS
350
360
370
J'α
B
Pro
Cys
His
Asn, Gly, Val
Ile
T206
R199
R210
D203
L202
E209
T207
V200
Pro
A205
L204
A201
V208